EurJIC European Journal of Inorganic Chemistry

ChemPubSoc Europe

FULL PAPER

DOI:10.1002/ejic.201402049

(Benzimidazolylmethyl)amine Zn^{II} and Cu^{II} Carboxylate Complexes: Structural, Mechanistic and Kinetic Studies of Polymerisation Reactions of ε-Caprolactone

Nelson W. Attandoh,[a] Stephen O. Ojwach,*[a] and Orde Q. Munro[a]

Keywords: Zinc / Copper / Ligand design / Ring-opening polymerization / Polymerization / Kinetics

Compounds *N*-(1*H*-benzimidazol-2-ylmethyl)aniline (**L1**), *N*-(1*H*-benzimidazol-2-ylmethyl)-2-bromoaniline (**L2**), and *N*-(1*H*-benzimidazol-2-ylmethyl)-2-aminothiophenol (**L3**) react with Zn^{II} and Cu^{II} carboxylates to form complexes $[Zn_2(\mathbf{L1})_2(OBn)_4]$ (**1**), $[Zn_2(\mathbf{L2})_2(OBn)_4]$ (**2**), $[Zn_2(\mathbf{L3})_2(OBn)_4]$ (**3**), $[Cu_2(\mathbf{L2})_2(OBn)_4]$ (**4**), $[Zn(\mathbf{L1})_2(OAc)_2]$ (**5**), $[Zn(\mathbf{L2})_2(OAc)_2]$ (**6**) and $[Cu_2(\mathbf{L1})_2(OAc)_4]$ (**7**). Structures of **2**, **4** and **6** revealed that **L1**–**L3** are monodentate, binding through the imidazolyl N-atom. The X-band EPR spectrum of **4** in the solid state is consistent with an antiferromagnetically-coupled (singlet) ground state and a low-lying EPR-active triplet excited state characterised by two main transitions. In dimethyl sulfoxide (DMSO) solution, a single resonance confirmed the retention of the dinuclear paddlewheel core. Complexes **1**–**7** formed active catalysts towards ring-opening polymerisation of ε-caprolactone. The polymerisation reactions follow first-order kinetics with respect to the monomer and occur through a coordination–insertion pathway.

Introduction

Transition-metal alkoxides have been employed as catalyst initiators for the ring-opening polymerisation (ROP) of cyclic monomers for decades.[1] Fine-tuning both the steric and electronic properties is essential for controlling both the activity and the nature of the polymers produced. For instance, increasing steric bulk of the ligand motif limits side reactions such as transesterification reactions.[2] These considerations have led to the design of a plethora of ligands containing single or multiple donors that are either monodentate, bidentate, or multidentate, depending on the ligand architecture and the identity of the metal atom.[3] A number of reviews detailing the use of metal complexes with different ligand architectures as catalyst initiators for the ROP of lactides and lactones have recently appeared in literature.[4] In addition to the ligand design, the choice of the metal centre has become an integral aspect in the ROP of cyclic esters due to their potential applications in biomedical and pharmaceutical fields.[5] As a result, the use of more biocompatible metals that display comparable activity to those of commercial tin-based catalysts[6] and other heavy metals is gaining momentum. Examples of such metal complexes include Ca,[7] Mg,[8] Fe,[1a] and alkali metals.[9] More recently, Zn^{II} and Cu^{II} metals have received appreciable attention as catalysts in the ROP of lactides and lactones due to their low toxicity, lower costs, and ease of synthesis.[10,11] For instance, Garces et al.[12] synthesised good molecular weight polymers (21000–34600 Da) with moderate polydispersity index (PDI; 1.09–1.53) by using heteroscorpionate amide zinc complexes, whereas Li et al.[13] employed a series of air-stable copper complexes supported on benzotriazole phenoxide ligands to synthesise polylactides with molecular weight as high as 28000 Da and molecular weight distribution in the range of 1.09–1.75.

As part of our contribution in this area, we recently reported the use of (pyrazolylmethyl)pyridine Zn^{II} and Cu^{II} complexes as catalysts in the ROP of ε-caprolactones.[14] In this context, we investigated the viability of using (benzimidazolyl)amine Zn^{II} and Cu^{II} complexes to catalyse ROP of ε-caprolactones. These ligands have recently attracted significant interest due to the nucleophilic imide N-atom,[15] in addition to their biocompatible nature.[16] Herein, we report the coordination chemistry of Zn^{II} and Cu^{II} carboxylate complexes with (benzimidazolyl)amine ligands and their applications in the ROP of ε-caprolactone. Detailed structural, kinetics and mechanistic studies of these polymerisation reactions have been performed and are discussed.

Results and Discussion

Synthesis and Structures of Zn and Cu Complexes

The (benzimidazolylmethyl)amine ligands, *N*-(1*H*-benzimidazol-2-ylmethyl)aniline (**L1**), *N*-(1*H*-benzimidazol-2-ylmethyl)-2-bromoaniline (**L2**), and *N*-(1*H*-benzimidazol-2-

[a] School of Chemistry and Physics, University of KwaZulu-Natal, Pietermaritzburg Campus, Private Bag X01 Scottsville, 3209, South Africa
E-mail: ojwach@ukzn.ac.za
http://chemistrypmb.ukzn.ac.za/StaffProfiles/DrStephenOjwach.aspx

Supporting information for this article is available on the WWW under http://dx.doi.org/10.1002/ejic.201402049.

ylmethyl)-2-aminothiophenol (**L3**) were synthesised by using a modified literature procedure (Scheme 1).[17] The compounds were obtained in moderate to good yields (51–71%) as pale-yellow solids.

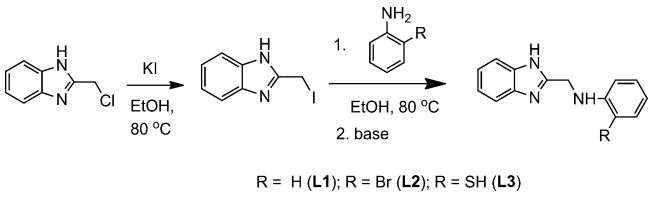

Scheme 1. Synthesis of ligands.

The corresponding bimetallic Zn^{II} and Cu^{II} benzoate complexes $[Zn_2(\mathbf{L1})_2(OBn)_4]$ (**1**), $[Zn_2(\mathbf{L2})_2(OBn)_4]$ (**2**), $[Zn_2(\mathbf{L3})_2(OBn)_4]$ (**3**), and $[Cu_2(\mathbf{L2})_2(OBn)_4]$ (**4**) were synthesised by a one-pot, two-step reaction (Scheme 2). Generation of the metal benzoate salts was achieved by reacting the appropriate metal acetate with two equivalents of benzoic acid. This was followed by addition of the appropriate ligand (**L1**–**L3**) in situ to afford the corresponding binuclear compounds in low to good yields (21–87%). The corresponding acetate complexes were prepared by reacting the Zn and Cu acetate salts with one equivalent of the appropriate ligand to produce complexes $[Zn(\mathbf{L1})_2(OAc)_2]$ (**5**), $[Zn(\mathbf{L2})_2(OAc)_2]$ (**6**), and $[Cu_2(\mathbf{L1})_2(OAc)_4]$ (**7**) in moderate yields (Scheme 3). Whereas the acetate Zn complexes **5** and **6** were monometallic in the solid state, the Cu complex **7** was bimetallic. The zinc and copper complexes were isolated as pale-yellow and pale-blue solids, respectively.

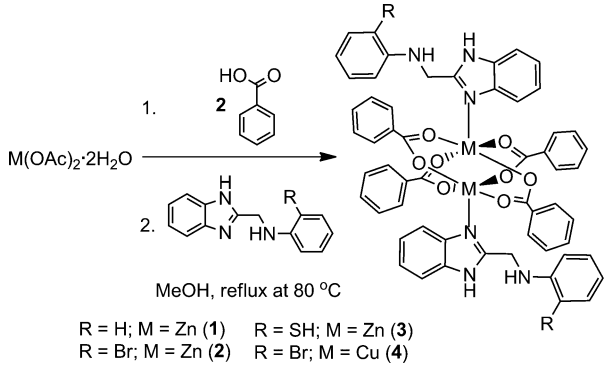

Scheme 2.

The identities of all the new compounds were established by using elemental analyses, mass spectrometry, IR spectroscopy, and single-crystal X-ray crystallography for complexes **2**, **4** and **6**. In addition, Zn complexes and paramagnetic Cu compounds were characterised by ^1H NMR spectroscopy and magnetic moment measurements, respectively. A notable feature in the ^1H NMR spectra of the ligands was the appearance of methylene protons as a doublet in **L2** as opposed to the singlet peaks recorded for **L1** and **L3**. ^1H–^1H COSY spectrum of **L2** (Figure S1) revealed the coupling of the methylene protons to the adjacent amine proton. This could occur because of the slow rate of exchange of N–H proton in the presence of the electron-withdrawing Br atom.[18] The ^1H NMR spectra of the Zn complexes exhibited slight shifts relative to those of the respective ligands, which was useful in deducing complex formation. For example, CH_2 signals for **L2** and **2** were observed at = 4.59 and 4.69 ppm, respectively.

Typical IR spectra of **L1**–**L3** and their corresponding complexes showed $\nu_{C=N}$ shifts to higher frequencies in the complexes. For example, the $\nu_{C=N}$ in **L3** shifted from 1595 to 1687 cm^{-1} in the corresponding complex **3**. This was diagnostic of coordination of the metal atoms to the nitrogen atom of the benzimidazolyl ring, consistent with previous reports.[19] The measured magnetic moments of the paramagnetic complexes **4** and **7** were 1.86 and 2.12 BM, respectively. The values fall within the range of Cu^{II} complexes containing Cu–Cu interaction.[20] The microanalyses data of all the complexes were consistent with the proposed structures in Schemes 1 and 2 and confirmed the purity of the compounds.

Solid-State Structures of Complexes 2, 4 and 6

Single crystals of **2**, **4** and **6** that were suitable for X-ray diffraction analyses were obtained by slow evaporation of methanol solutions of **2** and **4** and a dichloromethane solution of **6** at room temperature. Crystallographic data and structure refinement parameters are presented in Table 1, and Figures 1, 2 and 3 show the molecular structures of complexes **2**, **4** and **6**, respectively. The solid-state structures of **2** and **4** are dinuclear and exhibit inversion symmetry. The asymmetric unit in **2** and **4** comprises one metal centre, two benzoate anions, and one benzimidazolyl ligand. In

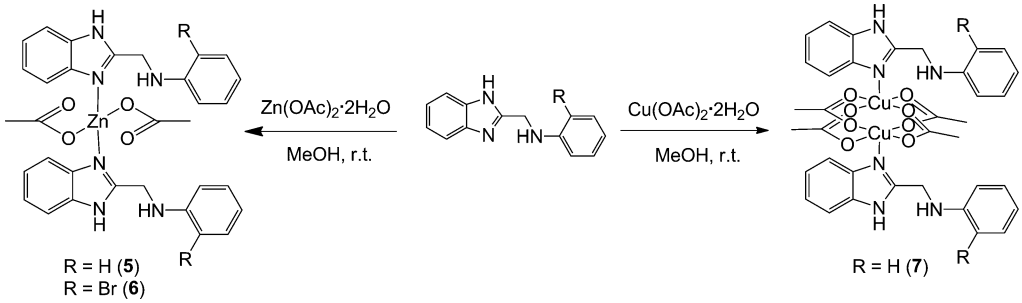

Scheme 3.

Table 1. Crystal data collection and structural refinement for complexes **2**, **4** and **6**.

	2	**4**	**6**
Chemical formula	$C_{56}H_{44}Br_2N_6O_8Zn_2{\cdot}2(CH_3OH)$	$C_{56}H_{44}Br_2Cu_2N_6O_8{\cdot}2(CH_3OH)$	$C_{32}H_{30}Br_2N_6O_4Zn$
Mr	1283.62	1279.96	787.81
Crystal system	triclinic	triclinic	triclinic
Space group	$P\bar{1}$	$P\bar{1}$	$P\bar{1}$
Temperature [K]	100	100	100
a [Å]	10.7836(15)	10.5718(7)	9.4041(6)
b [Å]	11.6897(16)	11.6594(7)	12.1658(8)
c [Å]	11.6997(16)	11.6631(7)	14.7332(9)
α [°]	74.925(8)	75.481(3)	103.670(3)
β [°]	82.395(8)	75.859(3)	102.615(3)
γ [°]	75.853(8)	82.766(3)	94.692(3)
V [Å^3]	1377.2(3)	1346.32(14)	1582.42(17)
Z	1	1	2
Radiation	Mo-K_α	Mo-K_α	Mo-K_α
μ [mm^{-1}]	2.39	2.34	3.35
Crystal size [mm]	0.38 × 0.35 × 0.25	0.20 × 0.20 × 0.15	0.10 × 0.10 × 0.10
Data collection			
Diffractometer	Bruker Apex II Duo	Bruker Apex II Duo	Bruker Apex II Duo
Absorption correction	Multi-scan *SADABS2012*/1 (Bruker, 2012)	Multi-scan *SADABS2012*/1 (Bruker, 2012)	Multi-scan *SADABS2012*/1 (Bruker, 2012)
$T_{min.}$, $T_{max.}$	0.771, 1.000	0.623, 0.746	0.654, 0.745
Measured, independent and observed [$I > 2\sigma(I)$] reflections	11291, 4843, 4391	23779, 6531, 5905	23107, 6113, 5574
R_{int}	0.021	0.018	0.018
Refinement			
$R[F^2 > 2\sigma(F^2)]$, $wR(F^2)$, *S*	0.023, 0.052, 1.05	0.034, 0.094, 1.07	0.021, 0.051, 1.06
Number of reflections	4843	6531	6311
Number of parameters	365	365	424
Number of restraints	1	0	0
$\Delta\rangle_{max}$, $\Delta\rangle_{min}$ [e Å^3]	0.31, –0.37	0.61, –1.21	0.37, –0.28

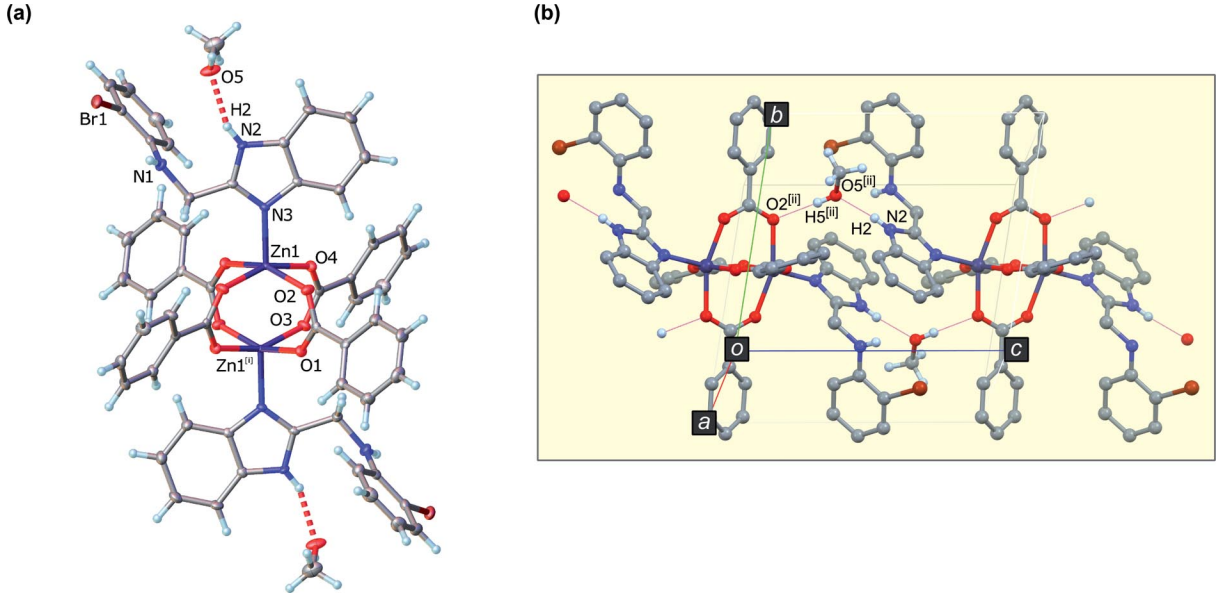

Figure 1. (a) View of the solid-state structure of **2** with thermal ellipsoids drawn at the 50% probability level. H atoms are rendered as spheres of arbitrary radii. Selected symmetry-unique atom labels are shown. Selected bond lengths [°] and angles [Å]: Zn1–Zn1[i] 3.0311(5), Zn1–O1 2.1164(14), Zn1–O2 2.0856(14), Zn1–O3 2.0268(14), Zn1–O4 2.0273(14), Zn1–N3 2.0195(16), N3–Zn1–O1 98.51(6), N3–Zn1–O2 102.90(6), N3–Zn1–O3 101.64(6), N3–Zn1–O4 101.30(6), O3–Zn1–O4 157.03(6), O3–Zn1–O2 87.84(6). (b) View of the one-dimensional hydrogen-bonded chain in the crystal structure of **2** showing two adjacent dinuclear complexes bridged by a pair of methanol solvent molecules; the chain axis is collinear with the *c*-axis. Symmetry codes: [i] 1 – *x*, 1 – *y*, 2 – *z*; [ii] *x*, 1 + *y*, *z*.

each molecule, the two metal centres are bridged by two pairs of benzoate ligands to form a paddlewheel structure. Complex **6**, on the other hand, is mononuclear and lacks inversion symmetry. The asymmetric unit contains the metal centre, two benzimidazolyl ligand units, and two metal-bound monodentate acetate ions.

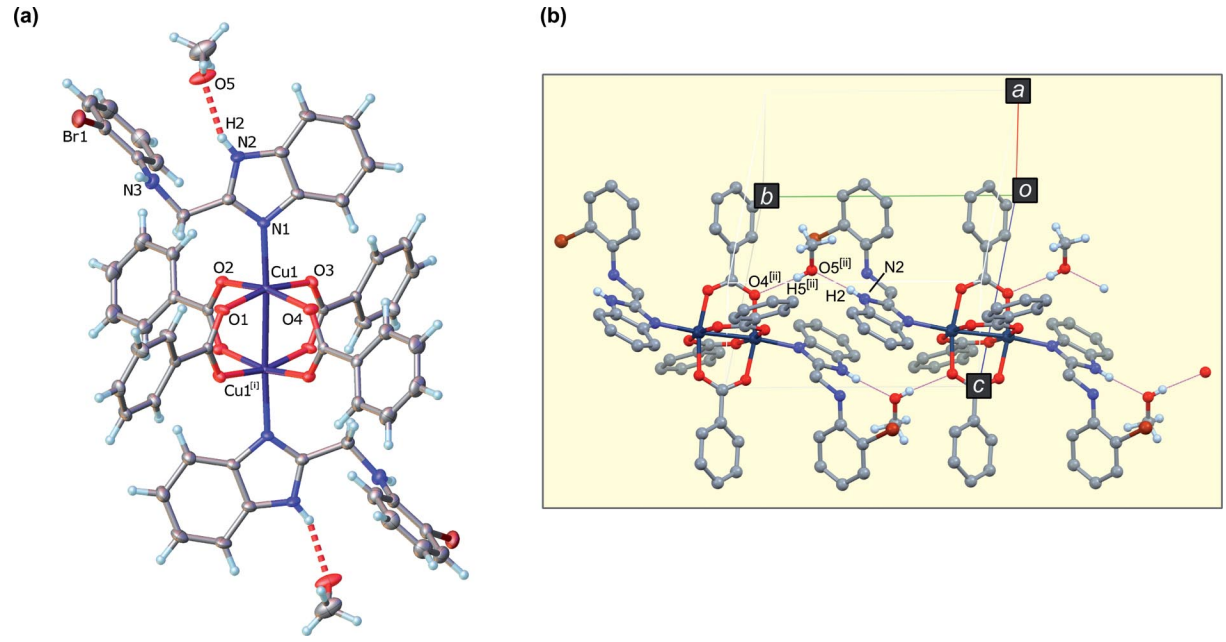

Figure 2. (a) View of the solid-state structure of **4** with thermal ellipsoids drawn at the 50% probability level. H atoms are rendered as spheres of arbitrary radii. Selected symmetry-unique atom labels are shown. Selected bond lengths [°] and angles [Å]: Cu(1)–N(1) 2.1390(19), Cu(1)–O(1) 1.9624(16), Cu(1)–O(2) 1.9970(16), Cu(1)–O(3) 1.9549(16), Cu(1)–O(4) 1.9891(17), Cu(1)–Cu(2) 2.6947(4), O(1)–Cu(1)–N(1) 96.62(7), O(2)–Cu(1)–N(1) 94.47(7), O(3)–Cu(1)–N(1) 96.84(7), O(4)–Cu(1)–N(1) 98.56(7), O(3)–Cu(1)–O(1) 166.48(7), O(1)–Cu(1)–O(2) 90.64(7). (b) View of the 1D hydrogen-bonded chain in the crystal structure of **4**; adjacent dinuclear complexes bridged by a pair of methanol solvent molecules are highlighted. The chain axis is collinear with the *b*-axis. Symmetry codes: [i] 1 – *x*, *y*, 2 – *z*; [ii] *x*, 1 + *y*, *z*.

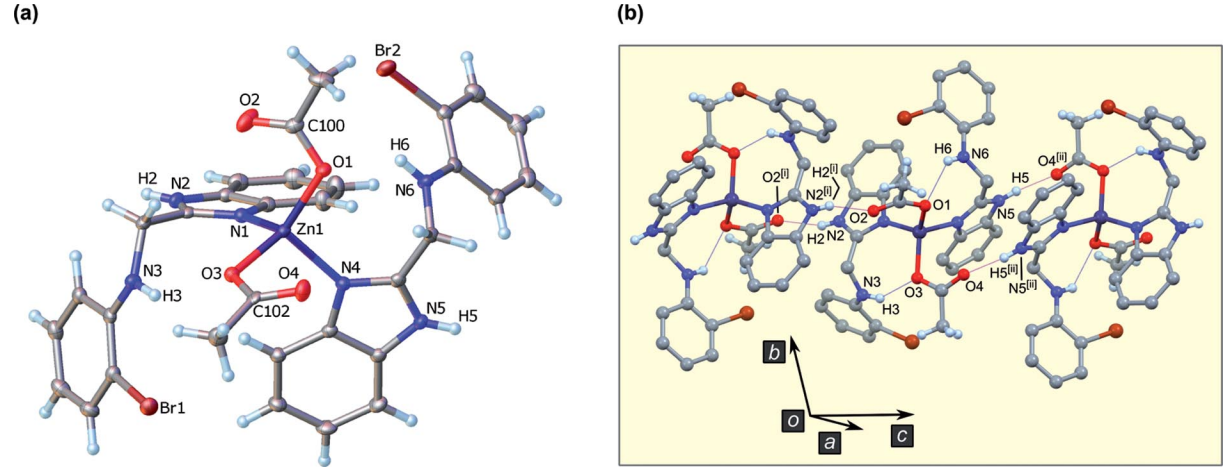

Figure 3. (a) View of the solid-state structure of **6** with thermal ellipsoids rendered at the 50% probability level. H atoms are depicted as spheres of arbitrary radii. Selected symmetry-unique atom labels are shown. Selected bond lengths [°] and angles [Å]: Zn(1)–O(3) 1.9708(13), Zn(1)–N(4) 2.0346(16), Zn(1)–N(1) 2.0277(17), Zn(1)–O(1) 1.9493(14), O(1)–Zn(1)–O(3) 117.84(6), O(1)–Zn(1)–N(4) 105.66(6), O(1)–Zn(1)–N(1) 118.81(6), N(1)–Zn(1)–N(4) 100.27(7). (b) View of the one-dimensional hydrogen-bonded chain in the crystal structure of **8**; both the intra- and intermolecular hydrogen bonds are highlighted. The chain axis is collinear with the [1,0,1] plane diagonal (i.e., the bisector of angle *aôc*). Symmetry codes: [i] – *x*, 2 – *y*, – *z*; [ii] 1 – *x*, 2 – *y*, 1 – *z*.

In the molecular and crystal structure of **2** (Figure 1), each Zn^{II} ion of the dinuclear compound is coordinated equatorially by four O-atoms of the bridging benzoate ligands and one axial nitrogen atom from **L2** to give a five-coordinate geometry. Although we initially anticipated a bidentate coordination mode for **L2**, the ligand in compound **2** coordinates in a monodentate fashion through the benzimidazolyl N-atom, whereas the secondary amine N–H functionality linking the aromatic ring systems of the ligand is noncoordinating. Interestingly, the trigonal planar nature of the secondary amine group (–CH_2–NH–Ar) suggests conjugation of the amine lone pair with the π-electron system of the aryl ring, possibly accounting for its apparently rather poor σ-donor strength and, hence, inability to facilitate chelation of the metal ion. The N–H groups of the benzimidazole ligands are, furthermore, hydrogen bonded

to the two solvent molecules (CH_3OH). The interaction metrics of the primary hydrogen bonding between **2** and the solvent are: N2–H2, 0.81(2) Å; H2···O5, 1.97(2) Å; N2–H2···O5, 157(2)°. The solvent hydroxy groups are further involved in bridging adjacent molecules in the lattice by donation of a hydrogen bond to a metal-bound benzoate oxygen atom (O2) of the neighbouring molecule. Because two such interactions exist for each molecule in the unit cell, one-dimensional hydrogen-bonded chains are formed in which pairs of methanol molecules effectively bridge pairs of dinuclear complexes (as shown in Figure 1, b). The chain axis is collinear with the *c*-axis of the unit cell. Because the chain propagates via the centre of inversion in the centre of the unit cell, it runs down the unit cell centre. The metrics of the secondary hydrogen bonds permitting this type of extended structure are: O5–H5A, 0.81(2) Å; H5A···O2,[ii] 1.98(2) Å; O5–H5A···O2,[ii] 177(2)° (symmetry code [ii]: *x*, 1 + *y*, *z*). The one-dimensional chains are additionally stabilised by π–π interactions between stacked benzimidazole rings of adjacent pairs of dinuclear complexes (the interplanar spacing measures 3.38 Å).

The Zn–O bond lengths in the equatorial plane remain in the range 2.0269(14) – 2.1164(14) Å, whereas the axial Zn–N bond length is 2.0195(16) Å; both are similar to those reported for other Zn^{II} complexes.[21] For example, the Zn–N bond length of complex **2** compares well with the distance of 2.02 Å reported for a single axially-coordinated N-atom,[22] but is shorter than the average Zn–N bond length of 2.10–2.11 Å reported for four-coordinate Zn^{II}[23] and the 2.15–2.19 Å bond length typical of six-coordinate Zn^{II}.[24] This is attributed to the extent of coordination around the metal centre.[25] The N–Zn–O bond angles subtended at the metal ion are inequivalent, averaging 101(2)°, and are consistent with a somewhat distorted square-pyramidal coordination geometry. The symmetry-related Zn^{II} ions are each displaced from the plane of their four coordinated oxygen atoms by 0.40 Å. The Zn···Zn distance between the two Zn atoms bridged by the four carboxylate groups is 3.0311(5) Å, similar to literature reports of other dimeric Zn^{II} complexes.[26] The observed metal-to-metal distance is greater than the sum of the van der Waal radii of Zn (1.39 Å),[27] consistent with the absence of any meaningful Zn–Zn interatomic metal bond. Each Zn^{II} ion is therefore five-coordinate with a distorted square pyramidal geometry.

In the dinuclear structure of **4** (Figure 2), each Cu^{II} ion is equatorially bonded to four oxygen atoms of the bridging carboxylate groups that form the paddlewheel core in a similar fashion to **2**. The structure of **4** is, likewise, centrosymmetric about an inversion centre located midway along the metal-to-metal interaction vector and a bis(methanol) solvate. As illustrated in Figure 2 (b), the extended structure of **4** is similar to that seen for **2**, with pairs of methanol molecules bridging dinuclear complexes by hydrogen bonds. The one-dimensional hydrogen bonded chains in **4**, however, run collinear with the *b*-axis rather than the *c*-axis (as found in **2**). Taken together, the molecular structures of **2** and **4** are essentially isomorphous, at both the molecular and supramolecular level. The interaction metrics of the hydrogen bonding between **4** and the solvent are: N2–H2, 0.77(3) Å; H2···O5,[ii] 2.01(3) Å; N2–H2···O5,[ii] 158(3)°; and O5[ii]–H5A,[ii] 0.74(5) Å; H5[ii]···O4,[ii] 2.12(5) Å; O5[ii]–H5A[ii]···O4,[ii] 175(5)° (symmetry code [ii]: *x*, 1 + *y*, *z*).

The four symmetry-unique Cu–O bond lengths range from 1.9549(16) to 1.9970(16) Å, averaging 1.976(20) Å. The imine-type nitrogen atoms of the pair of axial monodentate benzimidazole ligands effectively cap the paddlewheel core; the symmetry-unique Cu–N bond length measures 2.1390(19) Å. The mean Cu–O and Cu–N distances within the coordination group of **4** compare favourably with other related Cu^{II} complexes.[28] The O–Cu–O bond angles average 89(1)° and 166.7(3)° for the *cis*- and *trans*-angles, respectively. The Cu–Cu bond length of 2.6946(5) Å is within the normal range of 2.40–2.70 Å reported for related complexes.[29] The Cu^{II} ions of the paddlewheel core are displaced by 0.23 Å above the mean plane of the four metal-bound benzoate oxygen atoms. Collectively, the coordination geometry of each Cu^{II} ion is best described as a mildly distorted octahedron (taking into account the Cu–Cu bond).

In distinct contrast to the structures of **2** and **4**, the solid-state structure of the Zn^{II} derivative **6** is a mononuclear species in which the four-coordinate Zn^{II} ion binds two monodentate benzimidazole ligands (**L2**) and two monodentate acetate ions, thereby adopting a distorted tetrahedral coordination geometry (Figure 3). Each ligand is coordinated to the Zn^{II} ion through the benzimidazole imine-type nitrogen atom as observed in **2** and **4**. The Zn–N and Zn–O bond lengths average 2.031(5) and 1.960(15) Å, respectively, and compare well with other Zn^{II} complexes that display a similar coordination geometry.[30] The coordination group bond angles subtended at the Zn^{II} ion deviate significantly from the regular tetrahedral angle of 109.5°, consistent with a distorted tetrahedral geometry about the metal centre.

In the solid-state structure of **6**, each coordinated acetate oxygen atom (O1 and O3) is involved in an intramolecular hydrogen bond with the nearest aryl-appended N–H group of the neighbouring benzimidazolyl ligand, effectively locking in the observed orientation of the brominated aryl ring, at least in the solid state. The mean interaction metrics for the pair of intramolecular N–H···O hydrogen bonds are: N–H, 0.82(1) Å; NH···O, 2.284(7) Å; N–H···O, 139(4)°. The approximately trigonal planar geometry of the N–H donor groups of the ligands suggests substantial conjugation of the amine lone pair of electrons with the π electrons of the parent aryl ring and might contribute to the strength of the NH group as a hydrogen-bond donor in this case. Hydrogen bonding is, furthermore, significant in the supramolecular structure of **6**. Thus, although **6** does not form a solvated lattice, it forms one-dimensional hydrogen bonded chains akin to those in **2** and **4**, primarily as a result of centrosymmetric N–H···O hydrogen bonding involving the benzimidazole N–H donor in one molecule and the uncoordinated acetate oxygen atom of the neighbouring molecule. A complementary interaction completes the pair of centrosymmetric hydrogen bonds and generates an inversion pair, or H-

bonded dimer. Repetition of the hydrogen-bonding pattern along the cell diagonal (the line bisecting *aôc*) generates the 1D chain.

The interaction metrics of the hydrogen bonding within the 1D chains of **6** are: N2–H2, 0.79(3) Å; H2···O2,[i] 1.97(3) Å; N2–H2···O2,[i] 160(3)°; and N5–H5, 0.84(2); H5···O4,[ii] 1.86(2); N5–H5···O4,[ii] 171(3) (symmetry code [ii]: x, 1 + y, z). Interestingly, the intermolecular H···O distances in **6** are consistent with data reviewed by Steiner for N–H···O hydrogen bonds involving water as the acceptor and a range of N–H functional group donors (i.e., H···O interactions spanning the range 1.71–2.16 Å).[31]

Electron Paramagnetic Resonance (EPR) Analysis

The 295 K powder and solution phase (dimethyl sulfoxide, DMSO) X-band EPR spectra of the structurally-characterised Cu^{II} paddlewheel complex **4** are shown in Figure 4. The solid-state EPR spectrum of **4** is consistent with a dinuclear complex having two antiferomagnetically coupled Cu^{II} ions and a diamagnetic (singlet) ground state (S = 0) with a thermally accessible low-lying excited triplet state (S = 1). Because the g-tensors for the two excitations are of tetragonal symmetry (components x,$y \neq z$), the two spin-allowed $\Delta m_s = \pm 1$ transitions involving the excited triplet state levels (unpaired spins either $\uparrow\uparrow$, m_s = +1, or $\downarrow\downarrow$, m_s = –1, within the two Cu $d_{x^2-y^2}$ orbitals) are observed at 462 G (B_1^{xy} = 15.3) and 4878 G (B_2^{xy} = 1.45) as the primary (more intense) spectral features. The z-components of the two signals are more difficult to assign precisely, but possibly correspond to the features discernible at 1930 G (B_1^z) and 6308 G (B_2^z), completing the picture for the allowed triplet state transitions. The observed relation $g_n^{xy} < g_n^z$ for both transitions reflects axial compression of the g-tensors.

The grinding of polycrystalline **4** to record the powder EPR spectrum evidently caused some paddlewheel cleavage and the formation of a mononuclear Cu^{II} species (S = 1/2) characterised by the signal at g^{imp} = 2.09 (3372 G). This so-called "impurity" signal is commonly observed in the powder EPR spectra of dinuclear Cu^{II} paddlewheel derivatives and may be ignored when analysing the triplet state EPR spectrum. The powder EPR spectrum of **4** is very similar to those of the acetate-acetamido paddlewheel derivative $\{Cu_2(\mu_2\text{-}O_2CCH_3)_4\}(OCNH_2CH_3)$ recently studied in detail by Paredes-García et al.,[32] the dinuclear guanidinoacetic acid-bridged paddlewheel system reported by de Miranda et al.,[33] and the antiferromagnetically coupled dinuclear Cu^{II} paddlewheel-like compounds with 4-azabenzimidazole ligands reported by van Albada et al.[34] Consistent with the triplet-state spectra of other Cu^{II} paddlewheel derivatives, hyperfine coupling to the Cu nuclei (I = 3/2) within dinuclear **4** is not observed.

In solution, the EPR spectrum of **4** is almost perfectly isotropic and is characterised by a single line (g = 2.14), consistent with averaging of the zero-field splitting tensor, D, to zero as a result of random tumbling of the paddlewheel complex in solution. Such a situation renders the m_s = –1, 0, and +1 triplet-state levels degenerate in the absence of an applied magnetic field. In an applied magnetic field, the Zeeman splitting is symmetric, leading to equal spacings for the upper m_s = +1 and lower m_s = –1 states from the m_s = 0 state (barycentre). The spin-allowed $\Delta m_s = \pm 1$ transitions are thus degenerate and occur at a resonant frequency governed by g^{iso}. In the case of **4**, g^{iso} = 2.14; the significant g-shift relative to g_e (2.0023) reflects spin-orbit

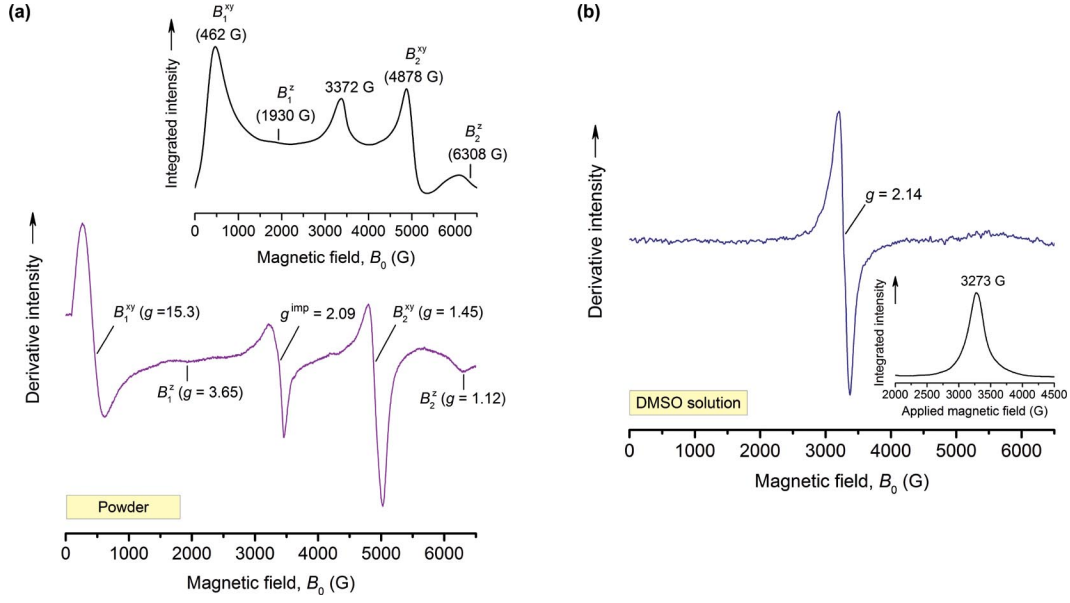

Figure 4. (a) Room temperature (295 K) powder EPR spectrum of **4** (microwave frequency, 9.870 GHz). (b) Room temperature EPR spectrum of **4** dissolved in DMSO (microwave frequency, 9.786 GHz). The inset spectra in both cases are the absorption spectra over the range encompassing the primary spectral features.

coupling effects in the paddlewheel complex. It is important to note that the absorption envelope for the signal in Figure 4 (b) is slightly anisotropic, or non-Lorentzian, with some asymmetry on the high-field side of the signal. This is possibly caused by the presence of the mononuclear impurity observed in the powder spectrum. That said, its contribution to the absorption profile in solution is essentially insignificant. The fact that a solution-phase signal for the triplet state of **4** is easily observed at room temperature suggests that the two spins are well-separated spatially and deftly confirms the vanishingly small magnitude of the zero-field splitting, *D*.

Polymerisation of ε-Caprolactone (ε-CL)

The catalytic activities of complexes **1**–**7** in the ROP of ε-caprolactone (ε-CL) were investigated in bulk at 110 °C. Table 2 contains a summary of the polymerisation data for complexes **1**–**7**. From preliminary investigations, it was evident that all the complexes exhibited significant catalytic activities in the ROP of ε-CL, achieving maximum conversion of about 95% between 48–96 h (Figure S2). These findings prompted us to perform detailed kinetics and mechanistic studies of these polymerisation reactions.

Table 2. ROP of ε-CL catalysed by complexes **1**–**5** and **7**.[a]

Entry	Cat.	*t* [h]	Conv. [%]	M_n (NMR)[b]	M_n (exp) [c]	PDI[c]	I*[d]
1	**1**	36	96	10906	3701	1.52	0.34
2	**2**	48	95	10857	3993	1.50	0.37
3	**3**	32	96	10960	2701	1.43	0.25
4	**4**	52	95	10843	4599	1.49	0.42
5	**5**	32	97	11078	4538	3.64	0.41
6	**7**	48	96	10983	3046	2.29	0.28

[a] Reaction conditions: 110 °C, [M]/[I] = 100, $[\varepsilon\text{-CL}]_o$ = 5.41 mmol, polymerisation of ε-CL in bulk. [b] Calculated from (M_w of monomer) × [M]/[I] × (% conv). [c] M_n(exp) = 0.56 × M_n(GPC). [d] Initiator efficiency = M_n(exp)/M_n(NMR).

Kinetics of ε-Caprolactone Polymerisation Reactions

The kinetics of the ROP of ε-CL catalysed by complexes **1**–**7** were investigated by monitoring the reaction profiles by ^{1}H NMR spectroscopy. The rates of the reaction were determined by plotting semilogarithm graphs of $\ln[CL]_0/[CL]_t$ vs. time (Figure 5). In all cases, induction periods were observed between 8–26 h. Reactions with copper catalysts showed longer induction periods compared with the analogous zinc complexes (Figure S3). Induction periods are usually associated with structural rearrangement/aggregation of the reacting species to form the active sites.[35] In this case, longer induction periods could imply significant differences between the active species and the catalyst precursors. However, linear relationships consistent with pseudo-first-order dependency on the monomer were observed after the induction periods (Figure 5), which is an indication that the generated active sites remained unchanged during the reaction profile. Thus, the rate of ε-CL polymerisation could be represented as depicted in Equation (1).

$$-\frac{d[CL]}{dt} = k_{app}[CL] \quad (1)$$

where $k_{app} = k_p[I]^x$, and where k_p is the chain propagation rate constant.

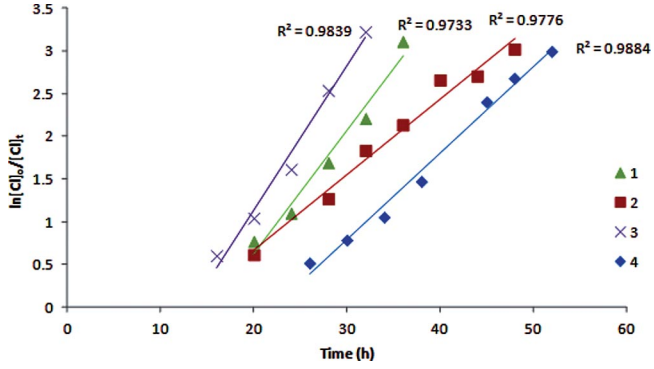

Figure 5. Plot of $\ln[CL]_0/[CL]_t$ vs. time showing linear fits after induction period for catalysts 1–4.

The apparent rate constants were extracted from the plots of $\ln[CL]_0/[CL]_t$ vs. time taking into account the induction period as 0.062 h^{-1} (**1**), 0.054 h^{-1} (**2**), 0.076 h^{-1} (**3**), 0.045 h^{-1} (**4**), 0.092 h^{-1} (**5**) and 0.027 h^{-1} (**7**). Thus Zn^{II} complexes exhibited higher catalytic activities compared with the corresponding Cu^{II} complexes. For example, rate constants of 0.054 and 0.045 h^{-1} were recorded for the analogous Zn^{II} and Cu^{II} complexes **2** and **4**, respectively. The higher catalytic activities of Zn^{II} complexes relative to their corresponding Cu^{II} complexes could be due to the higher electrophilicity of Zn^{II} metals making them better Lewis acids.[36] The ligand architecture also played a role in the catalytic activities of the complexes. For instance, complex **3** (0.076 h^{-1}) containing an –SH group was more active than the corresponding complex **2** (0.045 h^{-1}) bearing a Br^- group. Similar trends have been reported by Hodgson et al.[37] who found that replacement of an isopropyl group with a phenyl group on bis(thiophosphinic amine) resulted in a decrease in the rate constant from 9.50×10^{-3} to 1.57×10^{-3} s^{-1}. The identity of the carboxylate anion also had an effect on catalyst activity. Generally, acetate complexes afforded more active catalysts than the corresponding benzoate counterparts (Table 1, entries 1 vs. 5). This trend could be attributed to steric factors imposed by the bulky benzoate groups that limit monomer access to the metal centre.[38] We also observed greater catalytic activities for monomeric complexes in comparison to the corresponding dinuclear analogues (Table 2, entries 1 and 5). These results contrast with literature reports whereby multinuclear complexes generally form more active catalysts than mononuclear species.[1a] Our observation is consistent with stronger M–O bonds in the paddlewheel structures limiting dissociation to facilitate lactone monomer coordination. EPR data confirmed retention of the dimeric structure in solution and supports this hypothesis. Comparatively, the

observed rate constants of our complexes were lower than those of the most active zinc complexes reported in the literature.[39] However, they displayed comparable catalytic activities to zinc complexes reported by Chamberlain et al.[40] and aluminium alkoxide systems investigated by Zhong et al.[41]

To gain insight into the order of reaction with respect to the catalyst initiator and the subsequent overall order of the reaction, further kinetic studies were performed by using complex **1**. The order of the reaction was deduced from the gradient of the line of best fit of a plot of $\ln k_{app}$ vs. $\ln$[**1**] (Figure 6). From the plot, the order of the reaction with respect to catalyst **1** was obtained as 1.0085 ≈ 1. The overall order of the reaction could thus be described as second order according to Equation (2).

$$-\frac{d[CL]}{dt} = k_p[CL][\mathbf{1}] \quad (2)$$

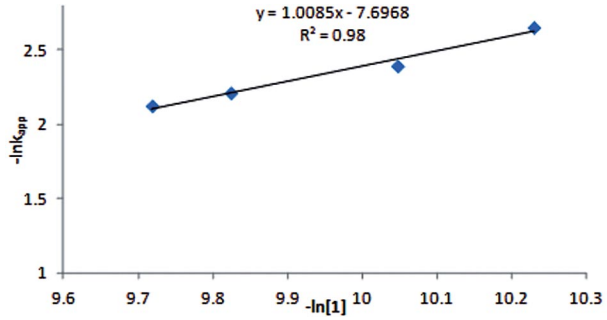

Figure 6. Plot of $\ln k_{app}$ vs. $\ln$[**1**] for the determination of order of reaction with respect to catalyst **1**.

Stability of Catalysts

The stability of the catalysts was investigated by the sequential addition of an equivalent amount of the monomer without addition of the catalyst, using complex **5**. This was done by addition of 100 equiv. of ε-CL after complete consumption of the monomer in the first cycle without adding the catalyst. The polymerisation kinetics proceeded to near completion, achieving 98% after 49 h (ε-CL) in the second cycle. The recorded k_{app} for the polymerisation kinetics dropped from 0.092 h^{-1} (1st cycle) to 0.073 h^{-1} (2nd cycle) corresponding to a 21% drop (Figure S4). It is therefore apparent that although the complexes remain significantly active in the second cycle, a loss of activity occurs. This is likely to originate from catalyst deactivation promoted by build-up of monomer impurities[2c] and/or thermal decomposition of the complex.[42]

Effect of Temperature and Solvent on the Polymerisation

The influence of temperature and solvent on the catalytic activities of complexes **2** and **4** are presented in Table 3. Decreasing the temperature from 110 to 60 °C resulted in a drastic decrease in rate constant from 0.056 to 0.007 h^{-1} (Table 3, entries 4–6). The use of methanol had a profound effect on the catalytic activity of complex **4**, affording a rate constant of 0.147 h^{-1} compared with a value of 0.045 h^{-1} obtained in the bulk experiment. Significantly, the activity recorded in toluene solvent was comparable to that in the bulk experiment (Table 3, entries 1–3). The significant increase in the catalytic activity of **4** in the presence of methanol could be due to generation of Zn-alkoxides (Zn-OCH_3) in situ, which are known to form highly active species in the polymerisation of cyclic esters as compared to metal acetates.[21c,43]

Table 3. Effect of temperature and solvent on the polymerisation of ε-CL by **2** and **4**.[a]

Entry	[I]	Solvent	T [°C]	M_n [g/mol]	PDI	k_{app} [h^{-1}][b]
1	**4**	bulk	110	4 599	1.49	0.045
2	**4**	toluene	110	5 102	1.58	0.053
3	**4**	methanol	110	1 530	1.29	0.147
4	**2**	bulk	110	3 993	1.50	0.056
5	**2**	bulk	90	2 554	1.42	0.030
6	**2**	bulk	60	–	–	0.007

[a] Reaction conditions: [M]/[I] = 100, [ε-CL] = 4.4 mmol. [b] k_{app} for the overall reaction including the induction period.

Molecular Weight and Molecular Weight Distribution

The molecular weight and molecular weight distribution (PDI) for PCL obtained by ROP catalysed by complexes **1**–**7** were determined by gel permeation chromatography (GPC) analyses and compared with their theoretical values computed on the basis of their ^{1}H NMR spectra. The molecular weight of the polymers ranged from 1847 to 4599 g/mol, corresponding to initiator efficiencies of between 25 and 42%. As an illustration, an experimentally determined molecular weight of 4538 g/mol was obtained for catalyst **5** at 97% compared with the expected theoretical molecular weight of 11078 g/mol. The polymers produced also exhibited moderate to broad PDI values in the range of 1.29 to 3.97. The broad molecular weight distributions coupled with low molecular weights of the polymer are indicative of transesterification reactions.[44] The poor initiating tenden-

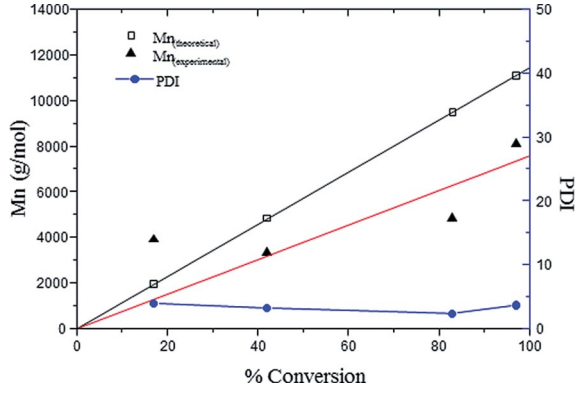

Figure 7. Plot of experimental and theoretical molecular weight against %conversion, showing the living polymerisation nature of catalyst **5**.

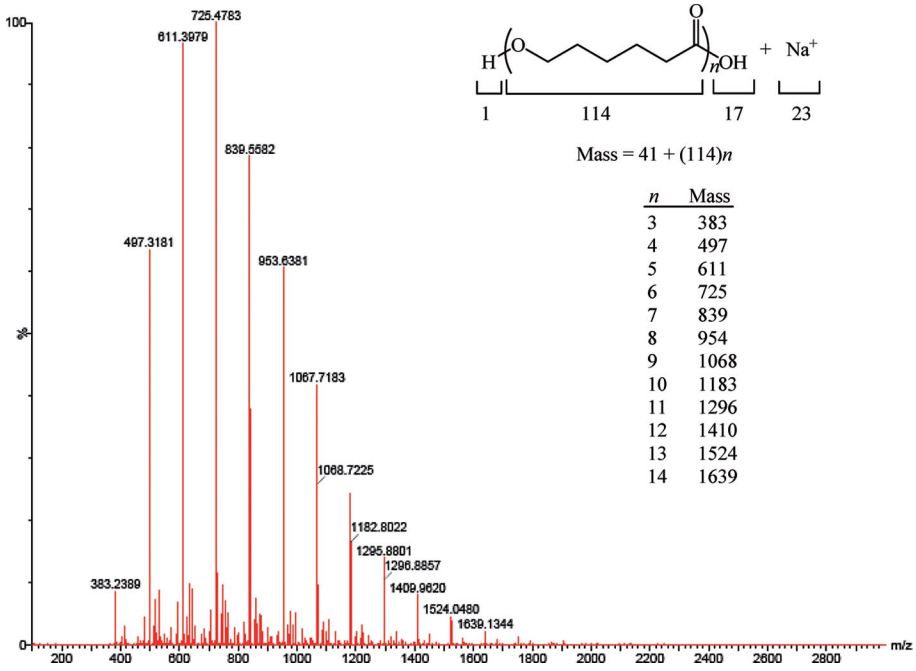

Figure 8. ESI-MS spectrum of crude polymer obtained by using catalyst **7** at 110 °C for 8 h. The presence of -OH end groups suggests hydrolysis of the acetate end groups.

cies of the carboxylate groups in relation to alkoxides may account for the lack of controlled polymerisation reactions.[3b,23] However, the reactions exhibited living polymerisation behaviour as demonstrated by the increase in molecular weight with percentage conversion in addition to the independence of PDI on percentage conversions (Figure 7).

Mechanism of ε-CL Polymerisation

The polymerisation of cyclic esters using Zn^{II} and Cu^{II} complexes is known to proceed through either a coordination insertion mechanism (CIM) or an activated-monomer mechanism (AMM).[45] To establish the mechanism of the ROP of ε-CL by catalysts **1**–**7**, a combination of ^{1}H NMR spectroscopy and mass spectroscopy was used to analyse the polymers obtained. The first-order dependency of the rates of polymerisation reactions on catalyst concentration (Figure 6) points to a coordination insertion mechanism. However, ^{1}H NMR spectra of the polymers obtained from **7** did not exhibit any signals associated with either the acetate or complex motifs (Figure S5). ESI-MS spectra of the polymers (Figure 8) showed fragments consistent with the presence of an –OH functionality [$HO(C_6H_{10}O)_nH{\cdot}Na^+$]. This could be due to the hydrolysis of the acetate and complex end-groups by adventitious water molecules[43,46] and might explain their absence in the ^{1}H NMR spectra. Thus, the polymerisation reactions of ε-CL by complexes **1**–**7** could be said to occur through a coordination-insertion pathway followed by hydrolysis of the acetate end groups.

Conclusion

We have demonstrated that (benzimidazolylmethyl)amine ligands adopt a monodentate coordination mode when reacted with zinc or copper carboxylates. Mononuclear and binuclear complexes are formed depending on the type of metal centre and the nature of the carboxylate ligand. EPR studies confirm that the paddle-wheel binuclear copper complexes are retained in solution. All the complexes form active catalysts for the ROP of ε-CL to produce low to moderate molecular weight polymers. The activities of these catalysts are dictated to a great extent by the nature of the metal centre and by the ligand architecture. The polymerisation kinetics were first order with respect to both monomer and catalyst and proceeded through a coordination-insertion mechanism. Despite the inferior catalytic behaviour of these complexes when compared with established zinc systems, they provide a convenient synthetic route to very stable catalysts. Moreover, the N–H functionality can be utilised to prepare discrete metal-alkoxide initiators that could offer better control of the polymerisation reactions.

Experimental Section

Materials and Measurements: All chemicals and solvents were purchased from Sigma–Aldrich and used as received. The monomer, ε-caprolactone was dried with CaH_2, vacuum distilled, and stored under inert conditions prior to use. Toluene was distilled from sodium, whereas methanol was purified by distillation from magnesium. NMR spectra were recorded with a Bruker 400 UltraShield NMR (400 MHz for ^{1}H and 100 MHz for ^{13}C) spectrometer. All

the chemical shifts are recorded in δ (ppm) relative to tetramethylsilane. The ^1H and ^{13}C NMR spectra are referenced using residual $CDCl_3$ and [D_6]DMSO solvent peaks, and the coupling constants (J) are reported in Hertz [Hz]. Elemental analyses were carried out with a Flash 2000 thermoscientific analyser. IR spectra were recorded with a Perkin–Elmer spectrum 100 series FTIR spectrometer. Mass spectra of the analytes were obtained with a micromass LCT premier mass spectrometer. The magnetic moments of paramagnetic copper complexes were determined with an Evans balance.

General Procedure for the Synthesis of Ligands: Equimolar amounts of 2-(chloromethyl)benzoimidazole, KI and amine were dissolved in ethanol (40 mL) and heated to reflux for 6 h at 80 °C. This was followed by addition of an equimolar amount of KOH and reflux was continued for a further 2 h. The reaction mixture was cooled to room temperature and poured into ice-cold water to give precipitates that were filtered and dried.

Ligand L1: 2-(Chloromethyl)benzoimidazole (1.67 g, 10.00 mmol), KI (1.66 g, 10.00 mmol), aniline (0.94 g, 0.92 mL, 10.00 mmol) and KOH (0.40 g, 10.00 mmol) were reacted to give **L1** (1.59 g, 71%) as a pale-yellow solid. ^1H NMR (400 MHz, $CDCl_3$): δ = 7.53 (dd, $^3J_{H,H}$ = 3.2 Hz, 2 H, ArH), 7.23 (dd, $^3J_{H,H}$ = 3.1 Hz, 2 H, ArH), 7.12 (dd, $^3J_{H,H}$ = 7.6 Hz, 2 H, ArH), 6.73 (t, $^3J_{H,H}$ = 7.3 Hz, 1 H, ArH), 6.60 (d, $^3J_{H,H}$ = 7.7 Hz, 2 H, ArH), 4.62 (s, 2 H, CH_2) ppm. ^{13}C NMR (100 MHz, $CDCl_3$): δ = 153.2 (C), 147.2 (C), 137.9 (C), 129.5 (CH), 122.8 (CH), 118.9 (CH), 114.9 (C), 113.2 (CH), 43.0 (CH_2) ppm. IR (KBr): $\tilde{\nu}$ = 3405 (s), 3050 (w), 1604 (s), 1510 (s), 1455 (m), 1421 (s), 1347 (w), 1318 (s), 1269 (s), 1183 (w), 1153 (w), 1106 (w), 1075 (w), 1011 (w), 996 (w), 928 (w), 875 (w), 875 (w), 838 (w), 745 (s), 692 (m) cm^{-1}. HRMS (ESI): *m*/*z* calcd for $C_{14}H_{13}N_3$ [M – H^+] 222.111; found 222.104.

Ligand L2: 2-(Chloromethyl)benzoimidazole (1.52 g, 9.14 mmol), KI (1.52 g, 9.14 mmol), 2-bromoaniline (1.57 g, 1.03 mL, 9.14 mmol) and KOH (0.52 g, 9.14 mmol) afforded **L2** (1.77 g, 64%) as a pale-yellow solid. ^1H NMR (400 MHz, [D_6]DMSO): δ = 7.44 (dd, $^3J_{H,H}$ = 1.7 Hz, 3 H, ArH), 7.14–7.11 (m, 3 H, ArH), 6.66 (dd, $^3J_{H,H}$ = 1.5 Hz, 1 H, ArH), 6.57–6.53 (m, 1 H, ArH), 4.59 (d, $^3J_{H,H}$ = 5.7 Hz, 2 H, CH_2) ppm. ^{13}C NMR (100 MHz, $CDCl_3$): δ = 153.3 (C), 145.2 (C), 132.7 (CH), 129.1 (CH), 118.3 (CH), 112.1 (CH), 109.3 (C), 42.2 (CH_2) ppm. IR (KBr): $\tilde{\nu}$ = 3426 (m), 2916 (w), 1595 (m), 1510 (m), 1456 (m), 1424 (m), 1399 (w), 1324 (w), 1311 (m), 1271 (m), 1220 (m), 1163 (w), 1097 (w), 1021 (m), 997 (w), 929 (w), 903 (w), 845 (w), 772 (s), 736 (s), 665 (w) cm^{-1}. HRMS (ESI): *m*/*z* calcd for $C_{14}H_{12}N_3Br$ [M^+] 302.169; found 302.029.

Ligand L3: 2-(Chloromethyl)benzimidazole (1.26 g, 7.55 mmol), 2-aminothiophenol (0.81 mL, 7.55 mmol), KI (1.25 g, 7.55 mmol) and KOH (0.43 g, 7.63 mmol) gave **L3** (1.20 g, 62.3%) as a pale-yellow solid. ^1H NMR (400 MHz, $CDCl_3$): δ = 7.52 (dd, $^3J_{H,H}$ = 3.2 Hz, 2 H, ArH), 7.31 (dd, $^3J_{H,H}$ = 1.5 Hz, 1 H, ArH), 7.23 (dd, $^3J_{H,H}$ = 3.2 Hz, 2 H, ArH), 7.14–7.10 (m, 1 H, ArH), 6.72 (dd, $^3J_{H,H}$ = 1.2 Hz, 1 H, ArH), 6.66–6.63 (m, 1 H, ArH), 4.21 (s, 2 H, CH_2) ppm. ^{13}C NMR (100 MHz, $CDCl_3$): δ = 151.7 (C), 148.4 (C), 138.5 (C), 136.3 (CH), 130.8 (CH), 122.6 (CH), 119.1 (CH), 116.6 (C), 115.4 (CH), 115.0 (CH), 32.9 (CH_2) ppm. IR (KBr): $\tilde{\nu}$ = 3358 (w), 3053 (w), 2743 (w), 1604 (s), 1531 (w), 1477 (s), 1432 (s), 1308 (m), 1272 (s), 1227 (m), 1139 (w), 1023 (m), 999 (w), 909 (w), 841 (w), 768 (m), 737 (s) cm^{-1}. HRMS (ESI): *m*/*z* calcd for $C_{14}H_{13}N_3S$ [M – H^+] 254.338; found 254.075.

Synthesis of Zn^{II} and Cu^{II} Complexes

$[Zn_2(L1)_2(OBn)_4]$ (1): A solution of $Zn(OAc)_2{\cdot}2H_2O$ (0.312 g, 1.42 mmol) and C_6H_5COOH (0.348 g, 2.85 mmol) in methanol (30 mL) was heated to reflux at 80 °C for 5 h followed by dropwise addition of **L1** (0.317 g, 1.42 mmol) in methanol (10 mL). The solution was heated to reflux for an additional 24 h, then the mixture was cooled to room temperature, filtered, and the solvent was removed under reduced pressure to afford a sticky yellow precipitate. The resulting yellow precipitate was dissolved in dichloromethane and the solvent was removed in vacuo to give **1** (0.577 g, 38%) as a pale-yellow solid. ^1H NMR (400 MHz, [D_6]DMSO): δ = 7.96 (d, $^3J_{H,H}$ = 7.4 Hz, 7 H, ArH), 7.50–7.39 (m, 13 H, ArH), 7.20 (br., 4 H, ArH), 7.01 (br., 2 H, ArH), 6.62–6.56 (m, 3 H, ArH), 6.36 (br., 1 H, ArH), 4.65 (s, 2 H, CH_2) ppm. ^{13}C NMR (100 MHz, $CDCl_3$): δ = 174.0 (CO), 148.3 (C), 134.5 (C), 131.8 (CH), 129.9 (CH), 129.3 (CH), 128.5 (CH), 123.2 (C), 122.4 (C), 117.5 (C), 113.1 (C), 22.0 (CH_2) ppm. IR (KBr): $\tilde{\nu}$ = 3034 (w), 1700 (br), 1602 (w), 1558 (br), 1403 (m), 1317 (w), 1220 (s), 1176 (w), 1070 (w), 1025 (w), 935 (w), 841 (w), 755 (s), 714 (m), 687 (m) cm^{-1}. $C_{56}H_{46}N_6O_8Zn_2{\cdot}0.5CH_2Cl_2$: calcd. C 61.45, H 4.29, N 7.61; found C 61.69, H 4.40, N 7.17.

$[Zn_2(L2)_2(OBn)_4]$ (2): $Zn(OAc)_2{\cdot}2H_2O$ (0.091 g, 0.415 mmol), C_6H_5COOH (0.101 g, 0.826 mmol) and **L2** (0.125 g, 0.415 mmol). Pale-yellow solid (0.319 g, 63%). Slow evaporation of methanol solution of **2** at room temperature gave pale-yellow crystals for X-ray diffraction analysis. ^1H NMR (400 MHz, DMSO): δ = 7.98–7.96 (m, 2 H, ArH), 7.64 (s, 1 H, ArH), 7.50–7.39 (m, 5 H, ArH), 7.15 (s, 2 H, ArH), 7.06 (s, 1 H, ArH), 6.65 (d, $^3J_{H,H}$ = 7.9 Hz, 2 H, ArH), 6.53 (t, $^3J_{H,H}$ = 7.1 Hz, 1 H, ArH), 5.99 (t, 1 H, NH), 4.69 (s, 2 H, CH_2) ppm. ^{13}C NMR (100 MHz, [D_6]DMSO): δ = 145.1 (C), 132.8 (CH), 129.9 (CH), 129.0 (CH), 128.4 (CH), 118.4 (CH), 112.1 (CH), 109.4 (C), 42.2 (CH_2) ppm. IR (KBr): $\tilde{\nu}$ = 3034 (w), 1687 (w), 1597 (w), 1558 (w), 1509 (w), 1453 (1383 w br), 1220 (s), 1022 (w), 931 (w), 843 (w), 772 (s), 710 (w), 684 (w) cm^{-1}. $C_{56}H_{44}Br_2N_6O_8Zn_2$: calcd. C 55.15, H 3.64, N 6.89; found C 55.43, H 3.83, N 7.06.

$[Zn_2(L3)_2(OBn)_4]$ (3): $Zn(OAc)_2{\cdot}2H_2O$ (0.095 g, 0.433 mmol), C_6H_5COOH (0.105 g, 0.859 mmol) and **L3** (0.110 g, 0.431 mmol). Pale-green solid (0.425 g, 87%). ^1H NMR (400 MHz, $CDCl_3$): δ = 8.07 (d, $^3J_{H,H}$ = 7.3 Hz, 1 H, ArH), 7.49 (t, $^3J_{H,H}$ = 7.4 Hz, 1 H, ArH), 7.36 (t, $^3J_{H,H}$ = 7.4 Hz, 1 H, ArH), 7.19–7.13 (m, 1 H, ArH), 6.98 (t, $^3J_{H,H}$ = 5.6 Hz, 1 H, ArH), 6.73–6.70 (m, 1 H, ArH), 6.58 (ddd, $^3J_{H,H}$ = 1.3, 1.4, 1.4 Hz, 1 H, ArH), 6.52 (s, 1 H, NH), 4.41 (s, 2 H, CH_2) ppm. ^{13}C NMR (100 MHz, $CDCl_3$): δ = 173.4 (CO), 148.6 (C), 136.8 (CH), 132.6 (CH), 132.3 (C), 131.6 (CH), 130.3 (CH), 128.2 (CH), 124.0 (C), 118.8 (C), 118.3 (CH), 115.3 (CH), 22.1 (CH_2) ppm. IR (KBr): $\tilde{\nu}$ = 3061 (br), 1705 (m), 1600 (s), 1559 (s), 1478 (w), 1448 (m), 1400 (s), 1314 (m), 1281 (m), 1250 (m), 1175 (m), 1158 (m), 1070 (m), 1048 (m), 1024 (m), 936 (w), 916 (w), 842 (m), 820 (w), 772 (m), 747 (m), 684 (m) cm^{-1}. $C_{56}H_{46}N_6O_8S_2Zn_2{\cdot}0.5CH_2Cl_2$: calcd. C 57.45, H 4.03, N 6.09; found C 57.48, H 4.34, N 6.32.

$[Cu_2(L2)_2(OBn)_4]$ (4): Compound **L2** (0.308 g, 1.02 mmol), $Cu(OAc)_2{\cdot}2H_2O$ (0.205 g, 1.03 mmol) and C_6H_5COOH (0.250 g, 2.05 mmol). Pale-green solid (0.512 g, 41%). IR (KBr): $\tilde{\nu}$ = 2831 (w), 2554 (w), 1684 (s), 1601 (m), 1573 (m), 1496 (w), 1453 (m), 1400 (s), 1324 (m), 1291 (s), 1178 (m), 1128 (w), 1072 (w), 1026 (w), 933 (m), 843 (w), 805 (w), 745 (m), 684 (m), 667 (m) cm^{-1}. $C_{56}H_{44}Br_2Cu_2N_6O_8{\cdot}0.5CH_2Cl_2$: calcd. C 53.93, H 3.60, N 6.68; found C 54.07, H 4.10, N 6.51. μ_{eff} = 1.86 BM.

$[Zn(L1)_2(OAc)_2]$ (5): To a solution of **L1** (0.24 g, 1.08 mmol) in methanol (5 mL) was added $Zn(OAc)_2{\cdot}2H_2O$ (0.24 g, 1.08 mmol) and the mixture was stirred at room temperature for 24 h. The solution was then evaporated under vacuum and the crude product was recrystallised from dichloromethane/hexane solvent mixture to afford complex **5** (0.27 g, 62%) as a pale-yellow solid. ^1H NMR

(400 MHz, [D$_6$]DMSO): δ = 6.3–7.7 (m, 9 H, ArH), 4.4 (s, 2 H, CH_2), 1.8 (s, 6 H, CH_3) ppm. MS (ESI): *m/z* (%) = 405 (5) [M^+], 346.04 (60) [$M^+ - C_2H_3O_2$], 223.11 (15) [$M^+ - C_4H_6O_4Zn$]. $C_{32}H_{32}N_6O_4Zn{\cdot}1.5CH_2Cl_2$: calcd. C 53.12, H 4.66, N 11.10; found C 52.98, H 4.83, N 11.17.

[Zn(L2)$_2$(OAc)$_2$] (6): To a solution of **L2** (0.13 g, 0.42 mmol) in methanol (5 mL), was added $Zn(OAc)_2{\cdot}2H_2O$ (0.092 g, 0.42 mmol) and the mixture was stirred at room temperature for 24 h. The solution was then evaporated under vacuum and the crude product was recrystallised from dichloromethane/hexane solvent mixture to afford complex **6** (0.13 g, 62%) as a pale-yellow solid. ^{1}H NMR (400 MHz, CDCL$_3$): δ = 7.6 (s, 2 H, Ar-H), 7.4 (s, 2 H, Ar-H), 7.3 (s, 2 H, Ar-H), 7.0 (s, 1 H, Ar-H), 6.5 (s, 2 H, Ar-H), 4.7 (s, 2 H, CH_2), 2.0 (s, 6 H, CH_3) ppm. $C_{32}H_{30}Br_2N_6O_4Zn{\cdot}CH_2Cl_2$: calcd. C 45.41, H 3.70, N 9.63; found C 45.92, H 3.73, N 9.67.

[Cu$_2$(L1)$_2$(OAc)$_4$] (7): This complex was prepared by dissolving **L1** (0.18 g, 0.82 mmol) and $Cu(OAc)_2{\cdot}2H_2O$ (0.16 g, 0.82 mmol) in methanol (10 mL) and stirring the mixture for 24 h at room temperature. The resulting precipitate was collected by filtration and washed with methanol to give **7** (0.22 g, 66%) as a pale-blue solid. ESI (MS): *m/z* (%) = 404 (20) [M^+], 345 (10) [$M^+ - C_2H_3O_2$]. $C_{18}H_{19}CuN_3O_4$ (404.91): calcd. C 53.39, H 4.73, N 10.38; found C 53.16, H 4.99, N 10.45. μ_{eff} = 2.12 BM.

Single Crystal X-ray Crystallography: Crystallographic data were collected with a Bruker APEX-II Duo CCD X-ray diffractometer with Mo-K_α radiation (λ = 0.7107 Å) at 100(2) K. Suitable crystals were selected and mounted in cryoprotectant oil with a 200 micron cryoloop (MiTEGen) for data collection. Data collection and processing employed the standard routines of the APEX-II program suit.[47] The data were corrected for absorption effects with SADABS.[48] Using Olex2,[49] the structure was solved with the ShelXS structure solution program by direct methods and refined with the ShelXL refinement package using cycles of least-squares minimisation.[50] All non-hydrogen atoms were refined anisotropically; H atoms involved in hydrogen bonds were located experimentally by using difference Fourier synthesis and refined isotropically.

CCDC-986363 (for **2**), -986364 (for **4**), and -986365 (for **6**) contain the supplementary crystallographic data for this paper. These data can be obtained free of charge from The Cambridge Crystallographic Data Centre via www.ccdc.cam.ac.uk/data_request/cif.

EPR Experiments: EPR spectra were recorded with a Bruker EMX-plus X-band spectrometer at 295 K. Solid crystalline **4** was ground into a fine powder and the spectrum was recorded by using the following parameters: microwave frequency: 9.870185 GHz; gain: 2.00×10^3; modulation amplitude: 5.0 G; conversion time: 37 ms; resolution: 3250 points; sweep width: 6500 G; 5 scans. The sample was then dissolved in DMSO and the solution phase spectrum was recorded in a quartz flat cell with the following data acquisition parameters: microwave frequency: 9.785709 GHz; gain: 2.00×10^3; modulation amplitude: 5.0 G; conversion time: 37 ms; resolution: 3250 points; sweep width: 6500 G; 5 scans.

General Procedure for Polymerisation of ε-Caprolactone: Polymerisation of ε-caprolactone was carried out in bulk at 110 °C. In a typical bulk polymerisation, 0.54 μmol of the complex was weighed into a pre-heated Schlenk tube equipped with a magnetic stirrer and ε-CL (0.60 mL, [M]/[I] = 100:1) was added. The Schlenk tube was immersed in a silicon oil bath at the desired temperature and the reaction mixture was stirred until completion of polymerisation. The extent of monomer conversions was monitored by taking aliquots at regular intervals and recording ^{1}H NMR spectra.

Polymerisation Kinetics: Kinetic studies were carried out by taking aliquots of the polymer at regular time intervals and quenching the reaction by freezing in liquid nitrogen. The quenched aliquots were dissolved in $CDCl_3$ and analysed by ^{1}H NMR spectroscopy. The ratio of initial monomer concentration to monomer concentration at time *t*, $[CL]_o/[CL]_t$, was determined based on the peak intensities of ε-CL and PCL from the ^{1}H NMR spectrum.[51] The signal around 4.2 ppm and 4.0 ppm corresponds to ε-CL and PCL, respectively.

Gel Permeation Chromatography: The molecular weight (M_w) and number average molecular mass (M_n) of the polymers were determined by Size Exclusion Chromatography (SEC) at Stellenbosch University. The SEC instrument consist of a Waters 1515 isocratic HPLC pump, Waters 717plus autosampler, Waters 600E system controller (run by Breeze version 3.30 SPA), a Waters in-line Degasser AF and a Waters 2414 differential refractometer (operated at 30 °C) in series with a Waters 2487 dual wavelength absorbance UV/Vis detector operating at variable wavelength. The polymers were dissolved in BHT-stabilised THF (2 mg/mL), filtered through 0.45 μm nylon filters and eluted through two sets of PLgel (Polymer laboratories) 5 μm Mixed-C (300 × 7.5 mm) column and a precolumn (PLgel 5 μm Guard, 50 × 7.5 mm) at a flow rate of 1 mL/ min. The column oven was kept at 30 °C and injection volume was 100 μL. THF (HPLC grade stabilised with 0.125% BHT) was used as the eluent. Narrow polystyrene standards ranging from 580 to 2×10^6 g/mol was used for calibration, hence, molecular weights were measured as polystyrene equivalents.

Supporting Informationormation (see footnote on the first page of this article)**:** Supplementary Figure S1 represents ^{1}H–^{1}H COSY spectra of **L2**; graphs of percentage conversions of monomer to PCL for catalysts **1**–**7** and induction periods are shown in Figures S2 and S3, respectively. A plot of $\ln[CL]_o/[CL]_t$ vs. time for the first and second cycle polymerisation reactions of ε-CL using complex **5** is given in Figure S4, and Figure S5 represents the ^{1}H NMR spectrum of crude polymers obtained from catalyst **5** after 8 h and 32 h.

Acknowledgments

The authors would like to thank the University of KwaZulu-Natal for financial support.

[1] a) B. J. O'Keefe, L. E. Breyfogle, M. A. Hillmyer, W. B. Tolman, *J. Am. Chem. Soc.* **2002**, *124*, 4384–4393; b) H.-Y. Chen, H.-Y. Tang, C.-C. Lin, *Macromolecules* **2006**, *39*, 3745–3752; c) C. K. Williams, L. E. Breyfogle, S. Kyung Choi, W. Nam, V. G. Young Jr., M. A. Hillmyer, W. B. Tolman, *J. Am. Chem. Soc.* **2003**, *125*, 11350–11359; d) P. J. Dijkstra, H. Du, J. Feijen, *Polym. Chem.* **2011**, *2*, 520–527.

[2] a) H.-Y. Chen, B.-H. Huang, C.-C. Lin, *Macromolecules* **2005**, *38*, 5400–5405; b) M. Cheng, D. R. Moore, J. J. Reczek, B. M. Chamberlain, E. B. Lobkovsky, G. W. Coates, *J. Am. Chem. Soc.* **2001**, *123*, 8738–8749; c) C. K. Williams, L. E. Breyfogle, S. K. Choi, W. Nam, V. G. Young Jr., M. A. Hillmyer, W. B. Tolman, *J. Am. Chem. Soc.* **2003**, *125*, 11350–11359; d) L. Azor, C. Bailly, L. Brelot, M. Henry, P. Mobian, S. Dagorne, *Inorg. Chem.* **2012**, *51*, 10876–10883; e) T. R. Jensen, C. P. Schaller, M. A. Hillmyer, W. B. Tolman, *J. Organomet. Chem.* **2005**, *690*, 5881–5891.

[3] a) K. Li, J. Darkwa, I. A. Guzei, S. F. Mapolie, *J. Organomet. Chem.* **2002**, *660*, 108–115; b) B. M. Chamberlain, M. Cheng, D. R. Moore, T. M. Ovitt, E. B. Lobkovsky, G. W. Coates, *J. Am. Chem. Soc.* **2001**, *123*, 3229–3238.

[4] a) R. H. Platel, L. M. Hodgson, C. K. Williams, *Polym. Rev.* **2008**, *48*, 11–63; b) C. M. Thomas, *Chem. Soc. Rev.* **2010**, *39*, 165–173; c) O. Dechy-Cabaret, B. Martin-Vaca, D. Bourissou,

Chem. Rev. **2004**, *104*, 6147–6176; d) I. dos Santos Vieira, S. Herres-Pawlis, *Eur. J. Inorg. Chem.* **2012**, 765–774.
[5] a) G. Parkin, *Chem. Rev.* **2004**, *104*, 699–767; b) V. Desai, S. G. Kaler, *Am. J. Clin. Nutr.* **2008**, *88*, 855–858.
[6] R. F. Storey, J. W. Sherman, *Macromolecules* **2002**, *35*, 1504–1512.
[7] M. H. Chisholm, J. Gallucci, K. Phomphari, *Chem. Commun.* **2003**, 48.
[8] a) J. Ejfler, M. Kobylka, L. B. Jerzykiewicz, P. Sobota, *Dalton Trans.* **2005**, 2047–2050; b) M. H. Chisholm, N. W. Eilerts, J. C. Huffman, S. S. Iyer, M. Pacold, K. Phomphrai, *J. Am. Chem. Soc.* **2000**, *122*, 11845–11854.
[9] J. Zhang, C. Jian, Y. Gao, L. Wang, N. Tang, J. Wu, *Inorg. Chem.* **2012**, *51*, 13380–13389.
[10] a) R. L. Arrowsmith, S. I. Pascu, H. Smugowski, *Organomet. Chem.* **2012**, *38*, 1–35, and references cited therein; b) C. K. Williams, N. R. Brooks, M. A. Hillmyer, W. B. Tolman, *Chem. Commun.* **2002**, 2132–2133; c) F. Drouin, P. O. Oguadinma, T. J. J. Whitehorne, R. E. Prud'homme, F. Schaper, *Organometallics* **2010**, *29*, 2139–2147.
[11] a) R. R. Gowda, D. Chakraborty, *J. Mol. Catal. A* **2010**, *333*, 167–172; b) A. John, V. Katiyar, K. Pang, M. M. Shaikh, H. Nanavati, P. Ghosh, *Polyhedron* **2007**, *26*, 4033–4044; c) S. Bhunora, J. Mugo, A. Bhaw-Luximon, S. Mapolie, J. Van Wyk, J. Darkwa, E. Nordlander, *Appl. Organomet. Chem.* **2011**, *25*, 133–145; d) J. Sun, W. Shi, D. Chen, D. Liang, *J. Appl. Polym. Sci.* **2002**, *86*, 3312–3315.
[12] A. Garces, L. F. Sanchez-Barba, C. Alonso-Moreno, M. Fajardo, J. Fernandez-Baeza, A. Otero, A. Lara-Sanchez, I. Lopez-Solera, A. Maria Rodriguez, *Inorg. Chem.* **2010**, *49*, 2859–2871.
[13] C.-Y. Li, S.-J. Hsu, C.-L. Lin, C.-Y. Tsai, J.-H. Wang, B.-T. Ko, C.-H. Lin, H.-Y. Huang, *J. Polym. Sci., Part A: Polym. Chem.* **2013**, *51*, 3840–3849.
[14] S. O. Ojwach, T. T. Okemwa, N. W. Attandoh, B. Omondi, *Dalton Trans.* **2013**, *42*, 10735–10745.
[15] W.-H. Sun, C. Shao, Y. Chen, H. Hu, R. A. Sheldon, H. Wang, X. Leng, X. Jin, *Organometallics* **2002**, *21*, 4350–4355.
[16] W. A. Craigo, B. W. LeSueur, E. B. Skibo, *J. Med. Chem.* **1999**, *42*, 3324–3333.
[17] a) K. C. S. Achar, K. M. Hosamani, H. R. Seetharamareddy, *Eur. J. Med. Chem.* **2010**, *45*, 2048–2054; b) H. Skolnik, A. R. Day, J. G. Miller, *J. Am. Chem. Soc.* **1943**, *65*, 1858–1862.
[18] R. M. Silverstein, F. X. Webster, D. J. Kiemle, *Spectrometric Identification of Organic compounds*, John Wiley & Sons, **2005**.
[19] M. S. Elder, G. A. Melson, D. H. Busch, *Inorg. Chem.* **1966**, *5*, 74–77, and references cited therein.
[20] M. Devereux, D. O'Shea, M. O'Connor, H. Grehan, G. Connor, M. McCann, G. Rosair, F. Lyng, A. Kellett, M. Walsh, D. Egan, B. Thati, *Polyhedron* **2007**, *26*, 4073–4084.
[21] a) S. Das, P. K. Bharadwaj, *Cryst. Growth Des.* **2006**, *6*, 187–192; b) H.-Y. Chen, H.-Y. Tang, C.-C. Lin, *Macromolecules* **2006**, *39*, 3745–3752; c) T. Jiang, X.-M. Zhang, *Cryst. Growth Des.* **2008**, *8*, 3077–3083.
[22] L. Qin, Y. Li, Z. Guo, H. Zheng, *Cryst. Growth Des.* **2012**, *12*, 5783–5791.
[23] C. C. Roberts, B. R. Barnett, D. B. Green, J. M. Fritsch, *Organometallics* **2012**, *31*, 4133–4141.
[24] P. Chaudhuri, C. Stockheim, K. Wieghardt, W. Deck, R. Gregrozik, H. Vahrenkamp, B. Nuber, J. Weiss, *Inorg. Chem.* **1992**, *31*, 1451–1462.
[25] X.-M. Chen, Y.-X. Tong, *Inorg. Chem.* **1994**, *33*, 4586–4588.
[26] a) L. Qin, Y. Li, Z. Guo, H. Zheng, *Cryst. Growth Des.* **2012**, *12*, 5783; b) N. Sreehari, B. Varghese, P. T. Manoharan, *Inorg. Chem.* **1990**, *29*, 4011–4015.
[27] A. Bondi, *J. Phys. Chem.* **1964**, *68*, 441–451.
[28] a) F. Bertolotti, A. Forni, G. Gervasio, D. Marabello, E. Diana, *Polyhedron* **2012**, *42*, 118–127; b) P. Drozdzewski, A. Brozyna, M. Kubiak, *THEOCHEM* **2004**, *707*, 131–137.
[29] a) M. Fan, Q. Yang, H. Tong, S. Yuan, B. Jia, D. Guo, M. Zhou, D. Liu, *RSC Adv.* **2012**, *2*, 6599–6605; b) V. M. Rao, D. N. Sathyanarayana, H. Manohar, *J. Chem. Soc., Dalton Trans.* **1983**, 2167–2173.
[30] a) B. Singh, J. R. Long, F. Fabrizi de Biani, D. Gatteschi, P. Stavropoulos, *J. Am. Chem. Soc.* **1997**, *119*, 7030–7047; b) U. Kumar, J. Thomas, R. Nagarajan, N. Thirupathi, *Inorg. Chim. Acta* **2011**, *372*, 191–199.
[31] T. Steiner, *Angew. Chem. Int. Ed.* **2002**, *41*, 48–76; *Angew. Chem.* **2002**, *114*, 50.
[32] V. Paredes-García, R. C. Santana, R. Madrid, A. Vega, E. Spodine, D. Venegas-Yazigi, *Inorg. Chem.* **2013**, *52*, 8369–8377.
[33] J. L. de Miranda, J. Felcman, M. H. Herbst, N. V. Vugman, *Inorg. Chem. Commun.* **2008**, *11*, 655–658.
[34] G. A. van Albada, I. Mutikainen, U. Turpeinen, J. Reedijk, *Polyhedron* **2006**, *25*, 3278–3284.
[35] a) J. L. Mata-Mata, J. A. Gutierrez, M. A. Paz-Sandoval, A. R. Madrigal, A. Martinez-Richa, *J. Polym. Sci., Part A: Polym. Chem.* **2006**, *44*, 6926–6942; b) Ph. Dubois, C. Jacobs, R. Jerome, Ph. Teyssie, *Macromolecules* **1991**, *24*, 2266–2270.
[36] L. M. Alcazar-Roman, B. J. O'Keefe, M. A. Hillmyer, W. B. Tolman, *Dalton Trans.* **2003**, 3082–3087.
[37] L. M. Hodgson, R. H. Platel, A. J. P. White, C. K. Williams, *Macromolecules* **2008**, *41*, 8603–8607.
[38] H.-Y. Chen, L. Mialon, K. A. Abboud, S. A. Miller, *Organometallics* **2012**, *31*, 5252–5261.
[39] a) H.-Y. Chen, B.-H. Huang, C.-C. Lin, *Macromolecules* **2005**, *38*, 5400–5405; b) D. J. Darensbourg, O. Karroonnirun, *Macromolecules* **2010**, *43*, 8880–8886; c) Y. Huang, W. Wang, C.-C. Lin, M. P. Blake, L. Clark, A. D. Schwarz, P. Mountford, *Dalton Trans.* **2013**, *42*, 9313–9324; d) J. Cayuela, V. Bounor-Legare, P. Cassagnau, A. Michel, *Macromolecules* **2006**, *39*, 1338–1346.
[40] B. M. Chamberlain, B. A. Jazdzewski, M. Pink, M. A. Hillmyer, W. B. Tolman, *Macromolecules* **2000**, *33*, 3970–3977.
[41] Z. Zhong, P. J. Dijkstra, J. Feijen, *J. Am. Chem. Soc.* **2003**, *125*, 11291–11298.
[42] O. Coulembier, C. Delcourt, Ph. Dubois, *Open Macromol. J.* **2007**, *1*, 1–5.
[43] A. Pilone, M. Lamberti, M. Mazzeo, S. Milione, C. Pellecchia, *Dalton Trans.* **2013**, *42*, 13036–13047.
[44] a) S. Song, H. Ma, Y. Yang, *Dalton Trans.* **2013**, *42*, 14200–14211; b) R. Petrus, P. Sobota, *Dalton Trans.* **2013**, *42*, 13838–13844.
[45] M. Labet, W. Thielemans, *Chem. Soc. Rev.* **2009**, *38*, 3484–3504.
[46] D. Bourissou, B. Martin-Vaca, A. Dumitrescu, M. Graullier, F. Lacombe, *Macromolecules* **2005**, *38*, 9993–9998.
[47] a) *Bruker-AXS*, Madison, Wisconsin, USA, **2009**; b) *SAINT*, *Area-Detector Integration Software*, Siemens Industrial Automation, Madison, WI, **1995**.
[48] *SADABS*, *Area-Detector Absorption Correction*, Siemens Industrial Automation, Madison, WI, **1996**.
[49] *OLEX2*, a complete structure solution, refinement and analysis program: O. V. Dolomanov, L. J. Bourhis, R. J. Gildea, J. A. K. Howard, H. Puschmann, *J. Appl. Crystallogr.* **2009**, *42*, 339–341.
[50] SHELX: G. M. Sheldrick, *Acta Crystallogr., Sect. A* **2008**, *64*, 112–122.
[51] Y. Ning, Y. Zhang, A. Rodriguez-Delgado, E. Y.-X. Chen, *Organometallics* **2008**, *27*, 5632–5640.

Received: February 12, 2014
Published Online: May 28, 2014

